

In vivo, label-free, three-dimensional quantitative imaging of kidney microcirculation using Doppler optical coherence tomography

Jeremiah Wierwille¹, Peter M Andrews², Maristela L Onozato³, James Jiang⁴, Alex Cable⁴ and Yu Chen¹

Doppler optical coherence tomography (DOCT) is a functional extension of optical coherence tomography (OCT) and is currently being employed in several clinical arenas to quantify blood flow *in vivo*. In this study, the objective was to investigate the feasibility of DOCT to image kidney microcirculation, specifically, glomerular blood flow. DOCT is able to capture three-dimensional (3D) data sets consisting of a series of cross-sectional images in real time, which enables label-free and non-destructive quantification of glomerular blood flow. The kidneys of adult, male Munich–Wistar rats were exposed through laparotomy procedure after being anesthetized. Following exposure of the kidney beneath the DOCT microscope, glomerular blood flow was observed. The effects of acute mannitol and angiotensin II infusion were also observed. Glomerular blood flow was quantified for the induced physiological states and compared with baseline measurements. Glomerular volume, cumulative Doppler volume, and Doppler flow range parameters were computed from 3D OCT/DOCT data sets. Glomerular size was determined from OCT, and DOCT readily revealed glomerular blood flow. After infusion of mannitol, a significant increase in blood flow was observed and quantified, and following infusion of angiotensin II, a significant decrease in blood flow was observed and quantified. Also, blood flow histograms were produced to illustrate differences in blood flow rate and blood volume among the induced physiological states. We demonstrated 3D DOCT imaging of rat kidney microcirculation in the glomerulus *in vivo*. Dynamic changes in blood flow were detected under altered physiological conditions demonstrating the real-time imaging capability of DOCT. This method holds promise to allow non-invasive imaging of kidney blood flow for transplant graft evaluation or monitoring of altered-renal hemodynamics related to disease progression.

Laboratory Investigation (2011) 91, 1596–1604; doi:10.1038/labinvest.2011.112; published online 1 August 2011

KEYWORDS: doppler optical coherence tomography (DOCT); glomerular blood flow; kidney microcirculation; optical coherence tomography (OCT)

Intrarenal hemodynamic abnormalities are thought to be a primary factor associated with the onset and progression of acute injury,¹ and other various nephropathies like diabetic nephropathy,^{2,3} and focal segmental glomerulosclerosis.⁴ Real-time assessment of renal morphological and hemodynamic changes could help to evaluate the kidney condition and offer valuable information to predict the prognosis of injury or disease leading to the development of patient-specific management strategies. Currently, there is no sensitive and objective tool for clinical monitoring of renal microcirculatory changes. The ability to monitor alterations in renal microcirculation due to vascular or glomerular disease may improve diagnostic and therapeutic interventions for renal health care.

Renal blood flow has been monitored using a number of different imaging modalities including positron emission tomography,^{5–10} and magnetic resonance angiography,^{11–14} Doppler ultrasound^{15–18} and contrast-enhanced ultrasound.^{19,20} Although these techniques allow for non-invasive, wide field-of-view imaging, they do not have sufficient resolution to detect changes in renal microcirculation (glomerular). Regarding kidney transplantation, studies have suggested that blood perfusion within glomerular capillaries may be correlated with intermediate and long-term graft function.^{21,22} Therefore, immediate detection of microcirculatory changes could provide decisive criteria for therapeutic interventions promoting graft salvage and long-term function.^{22–24}

¹Fischell Department of Bioengineering, University of Maryland, College Park, MD, USA; ²Department of Biochemistry, Georgetown University, Washington DC, USA; ³Department of Pathology, Massachusetts General Hospital, Harvard Medical School, Boston, MA, USA and ⁴Thorlabs, Inc, Newton, NJ, USA
Correspondence: Dr Y Chen, PhD, Fischell Department of Bioengineering, University of Maryland, 2218 Jeong H. Kim Building, College Park, MD 20742, USA.
E-mail: yuchen@umd.edu

Received 3 February 2011; revised 13 May 2011; accepted 4 June 2011

Optical imaging techniques that have higher resolutions and greater sensitivities could be a more feasible method for monitoring and evaluating microcirculatory changes, especially in an intraoperative setting. Several optical imaging techniques have been employed to study renal blood flow. Studies using confocal^{25–27} and multi-photon microscopy^{28–30} have demonstrated the ability to image kidney microstructure and function (blood flow and filtration rate) on animal models, but the penetration depth has been limited to several hundreds of microns,³¹ and they require the need to administer contrast agents to determine flow. Therefore, using these imaging modalities for human studies poses certain challenges due to the capsule surrounding the human kidney, which can be several hundreds of micrometers thick, and the need to inject contrast agents into the patient.

Optical coherence tomography (OCT)³² and its functional extension Doppler OCT (DOCT)³³ are emerging imaging technologies that have the capacity to provide real-time images (ie, immediate imaging) of tissue in a non-invasive fashion (ie, non-destructively) with high resolution near that of conventional histopathological images. Previous studies by us have demonstrated the ability of OCT to resolve renal corpuscles and uriniferous tubules³⁴ and evaluate the real-time morphological changes in these structures associated with ischemia-reperfusion injury *in vivo*.³⁵ Also, we have previously demonstrated that OCT can penetrate the kidney capsule surrounding human kidneys thereby enabling the characterization of renal tubules, glomeruli, and cortical blood vessels in human kidneys.^{36,37} OCT represents a light echo microscopy and has the potential to become a powerful tool for functional optical renal biopsy in the near future.³⁸

High-speed, Fourier-domain DOCT can be used to visualize blood flow non-invasively by measuring Doppler frequency shifts in the OCT interference signal caused by moving scatterers that are label free, such as red blood cells.³⁹ DOCT has been used to image and quantify blood flow *in vivo* for multiple clinical applications including retina,^{40–43} skin,^{44–46} and gastrointestinal tract,⁴⁷ among others.

In the present study, our objective was to demonstrate the feasibility of using DOCT to observe microcirculation within living kidneys in real time and quantitatively compare physiologically induced changes.

MATERIALS AND METHODS

OCT and DOCT

A high-speed, high-resolution OCT system was used in this study. The details of the OCT system have been previously described.³⁶ Briefly, a Fourier-domain OCT system consisting of a swept-source laser with 100 nm bandwidth at 1310 nm center wavelength yielding an axial resolution of $\sim 10 \mu\text{m}$ in tissue was used. A $10\times$ objective (Olympus Plan N, NA = 0.25) was used in the sample arm to achieve a lateral resolution of $\sim 2\text{--}3 \mu\text{m}$ determined by a USAF resolution target. The laser source operated at a sweep rate of

16 kHz allowing a series of two-dimensional cross-sectional images to be captured in real time to form a three-dimensional (3D) data set (voxel size: 1024 [X] by 256 [Y] by 512 [Z] pixels; dimension: 0.280 mm [X] by 0.325 mm [Y] by 1.90 mm [Z]; acquisition time <20 sec). OCT fringe data were acquired to obtain both amplitude and phase information after Fourier transform, and DOCT signals were computed using standard phased-resolved algorithm.³⁹

Animal Model and Preparation

The animal protocol has been approved by the committees on animal care and use in both the University of Maryland and Georgetown University. Male Munich–Wistar rats ($n = 3$, ~ 400 g) were used in this study. This strain of rat has numerous superficial glomeruli in the outer cortex that are accessible for observation.⁴⁸ Rats were regularly fed normal rat chow with free access to water at all times. During the study, rats were anesthetized by intraperitoneal injection of pentobarbital sodium (50 mg/kg body weight) and monitored routinely by tactile stimulation with supplemental anesthetic added as needed to maintain initial depth of anesthesia. After being secured on a portable surgical apparatus, the left kidney was exposed through laparotomy of the left flank region and the kidney was securely placed in a lucite holder. The right femoral vein was then cannulated with polyethylene tubing for administration of pharmacologic agents. Rats were then placed beneath the DOCT microscope for *in vivo* imaging. To induce alterations in renal blood flow, 0.1–0.2 ml mannitol (250 mg/ml), which increases renal blood flow,^{49–51} and 200 $\mu\text{g}/\text{kg}$ body weight angiotensin II,⁵² which decreases renal blood flow,^{53–56} were administered by a bolus injection into the femoral vein. Three injections of mannitol at 45 min intervals were performed followed by DOCT imaging after each injection and then a final injection of angiotensin II was given 10 min after the third mannitol injection and then followed by DOCT imaging. DOCT imaging was also performed $\sim 15\text{--}20$ min after each infusion of mannitol when the physiologic effects of the drug were diminishing. Data taken during this period are labeled ‘recover’ to distinguish it from the data taken immediately after each mannitol injection. At each stage, multiple glomeruli ($n \geq 3$) from different locations were imaged. Thus, the same glomeruli were not re-imaged at each stage.

OCT/DOCT Image Processing and Quantification

Glomeruli were located by scanning the surface of the cortex, and 3D data sets, including the fringe data for Doppler analysis, were acquired for each glomerulus (total $n = 44$). OCT intensity images as well as DOCT images were computed from the fringe data for each frame in the 3D data sets.⁵⁷ Quantification of single glomerular microcirculation parameters was performed offline using a custom image analysis program written in Matlab (Mathworks, Natick, MA, USA).

The glomerular volume (GV) was computed from the OCT intensity image according to the equation

$$GV = \frac{2}{3} S_A h \quad (1)$$

where S_A is the surface area through the mid-section of the glomerulus and h is the height of the glomerulus. The surface area and height of each glomerulus were manually selected by encircling the perimeter of the glomerulus in cross-sectional and *en face* images passing through the center of the glomerulus. The $2/3$ scaling factor converts the cylindrical geometry of the calculation to the more realistic elliptical or spherical geometry of glomeruli.

All 3D DOCT data were subsequently analyzed by computing cumulative Doppler volume and Doppler flow range (DFR) parameters. The cumulative Doppler volume (CDV)

was calculated by summing together the volume of segmented voxels within the GV containing DOCT signals that were above the background threshold as defined below in Eq. 2, where $V(x,y,z)$ is individual voxel volume.

$$CDV = \sum_{xyz} V(x,y,z) \quad (2)$$

The threshold value ($|v_z| = 0.05$ mm/s) for computing CDV was set to slightly above the average DOCT signal from regions of static tissue. The CDV is not equivalent to 'blood volume' as DOCT is only sensitive to scatterers (red blood cells). Therefore, the CDV we measured is expected to be smaller than actual 'blood volume' and is coupled with the level of hematocrit.

DFR was defined as the flow rate at 99% area under the curve (AUC) of the 3D flow histogram (see Figure 4). The

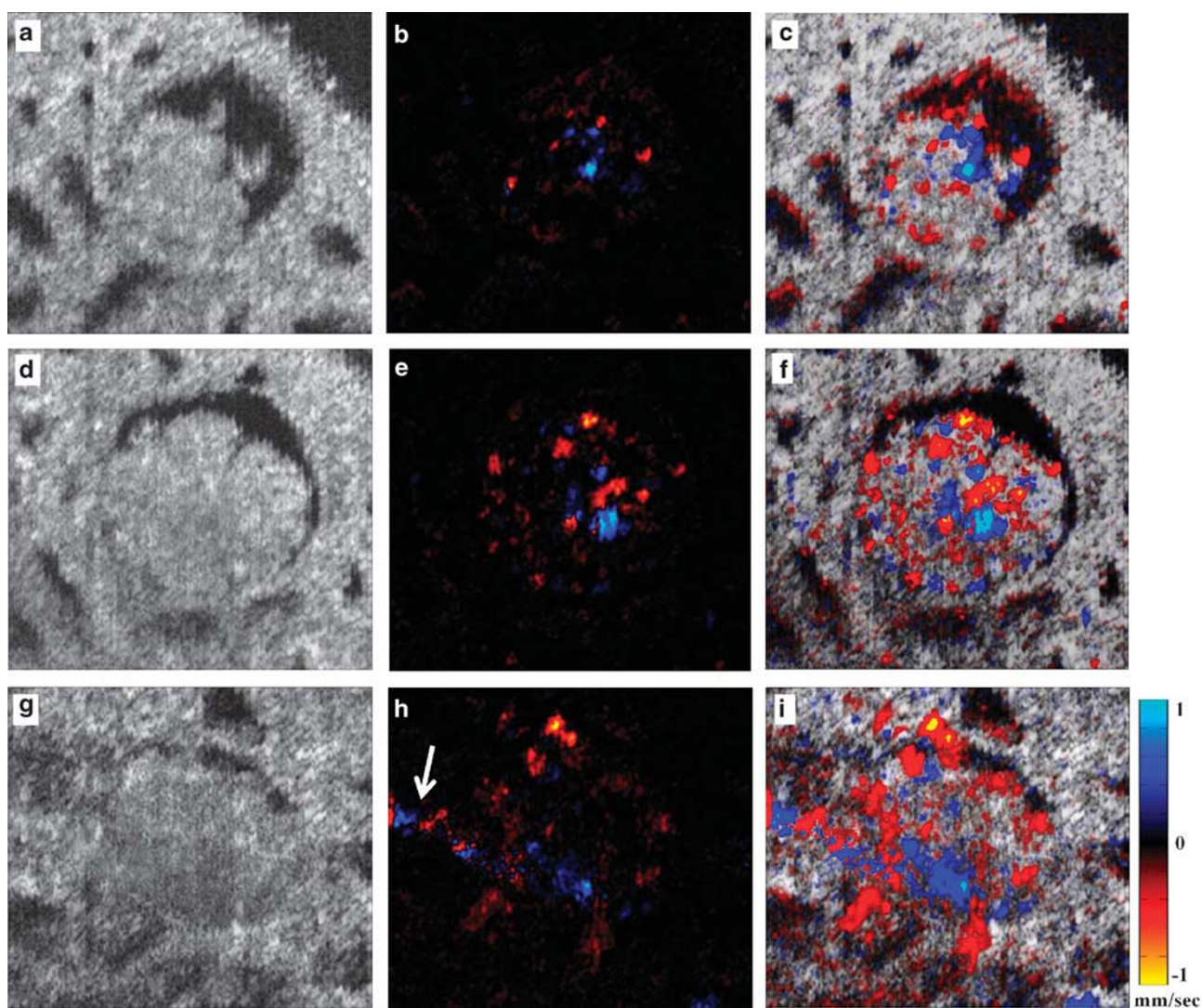


Figure 1 OCT and DOCT imaging of rat glomerulus. (a, d, g) OCT *en face* view of single glomerulus. (b, e, h) DOCT *en face* view of the same glomerulus. (c, f, i) Fused OCT/DOCT image showing spatial agreement between the OCT image and the corresponding DOCT image. The three images in each row correspond to the same imaging plane in depth. Depth (a–c) = 440 μm ; (b–f) = 470 μm ; (g–i) = 545 μm ; Image size: 325 \times 278 μm . See Supplementary Video 1 for entire 3D OCT/DOCT sectioning of the glomerulus.

omission of the last percentile was to reduce variability from outliers in the histogram that would significantly alter the flow range determination. 3D flow histograms were calculated by integrating the DOCT signal over the lateral cross-section (*en face*) area of the segmented capillaries within the GV at each depth position. Integration over the *en face* plane eliminates the angle-dependent uncertainty of the Doppler velocity, therefore providing an accurate quantitation of flow as defined in Eq. 3 below.⁵⁸ Doppler flow calculations were performed in *en face* images according to Eq. 3, where $v_z(x,y,z)$ is the segmented DOCT velocity according to a threshold of 0.05 mm/s integrated over the xy segmented DOCT area.

$$\text{Flow} = \int_x \int_y v_z(x, y, z) dx dy \quad (3)$$

Statistical Analysis

Data is given as mean \pm s.d. One-way ANOVA test was performed to evaluate sampling variance followed by Tukey's multiple comparison test with respect to the 'baseline' values to determine statistical significance ($P < 0.05$ were considered significant). All histograms were computed using consistent bin size of $5 \times 10^{-6} \mu\text{l/s}$ and minimum threshold equal to 0.05 mm/s.

RESULTS

After the rat left kidney was exposed beneath the microscope, several glomeruli were located by scanning the beam across the surface of the kidney. 3D data sets of glomeruli were acquired and stored for subsequent analysis. With PIP (picture-in-picture) mode enabling simultaneous OCT/DOCT on-screen viewing, we were able to see blood flow in each glomerulus in real time while scanning the surface of the kidney. OCT/DOCT-fused images were constructed offline to verify the spatial correlation of the captured DOCT signal. OCT/DOCT imaging of kidney glomerulus revealed intra-glomerular blood flow from the internal capillary network. Figure 1 shows images of three *en face* planes at different depths in a representative glomerulus: the top row is the upper region (a–c), the middle row is the middle region (b–f), and the bottom row is the lower region (g–i). Figures 1a,d and g show OCT intensity images revealing the kidney microstructure. Uriniferous tubules are readily identified surrounding the glomerulus, which is the circular structure in the middle of the image that surrounded by the crescent-shaped capsular space of Bowman. Figures 1b,e and h show corresponding DOCT images from the same plane depicting red blood cell velocity in numerous glomerular capillaries. As indicated by the colormap scale, red to yellow represents increasing velocity of blood flow in one direction whereas blue to cyan represents increasing velocity of blood flow in the opposite direction. Therefore, the mixture of these colors seen in the DOCT images demonstrates the varying velocities

as well as the convoluted nature of blood flow through the glomerular capillaries. Figures 1c,f and i are the fused OCT/DOCT images demonstrating the spatial location of the DOCT signal within the glomerulus seen in the OCT images. 3D OCT/DOCT images sectioning through the entire GV are shown in Supplementary Video 1. DOCT clearly visualizes the vascular pole showing the afferent or efferent arteriole (Figure 1h, arrow). Note that this imaging information is not readily apparent in the corresponding OCT structure image. Figure 2a shows a top-down view of the complete 3D DOCT signal captured from the glomerulus in Figure 1 where the vascular pole with an arteriole is readily identified (arrow). Figure 2b offers a 3D perspective of the OCT/DOCT signal from the same glomerulus. The grayscale colormap represents the segmented OCT structural image showing renal tubules and Bowman's space, and the red/blue

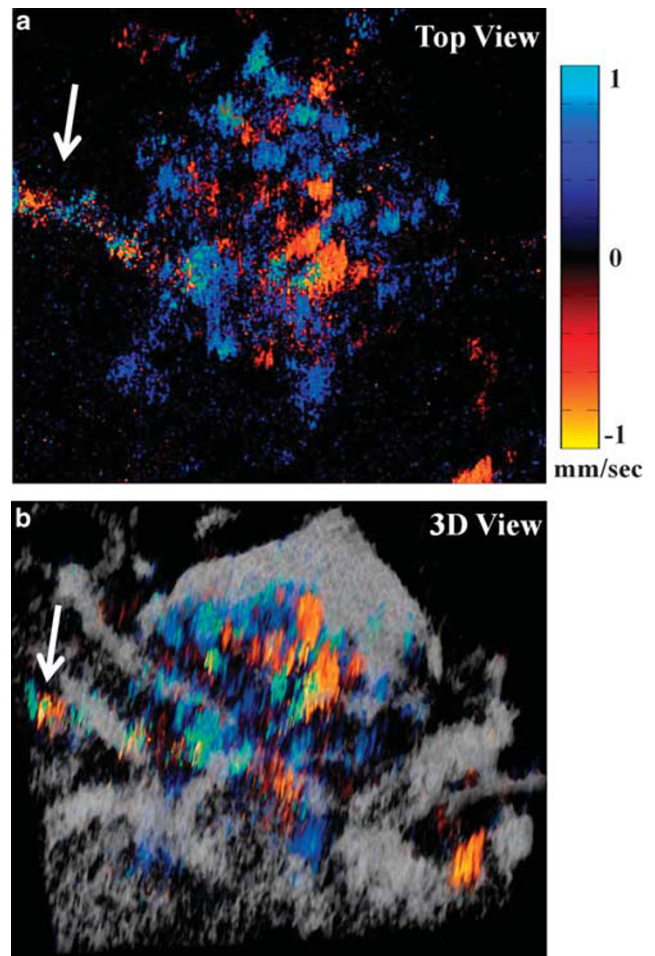


Figure 2 (a) Top-down (*en face*) view showing numerous clustered DOCT signals within the glomerulus representing red blood cell velocities. Image size: $325 \times 278 \mu\text{m}$. (b) Three-dimensional (3D) rendering of the 3D OCT/DOCT data set of the glomerulus in Figure 1 reconstructed from a series of cross-sectional images (see Supplementary Video 2). Grayscale colormap represents segmented kidney microstructures from OCT and red-blue colormap represents bi-directional blood velocity from DOCT. Volume size: $325 \times 278 \times 580 \mu\text{m}$.

colormap represents the DOCT signal. Beneath the broad, gray, umbrella-like structure (Bowman's space) is the glomerulus interior where numerous DOCT signals nest together representing the blood flow in capillary tufts (see Supplementary Video 2 with 3D camera rotation to enable viewing from different perspectives).

In vivo DOCT imaging was performed during three separate physiological states: baseline, following injection of

mannitol, and following injection of angiotensin II. Figure 3 shows representative glomeruli imaged under each condition. Baseline DOCT is depicted in Figure 3b with mannitol and angiotensin II in Figures 3d and f, respectively. The increase or decrease of the DOCT signal is readily visible following administration of mannitol or angiotensin II, respectively. Corresponding OCT images are presented in Figures 3a,c and e for identification of glomerular region in the DOCT images.

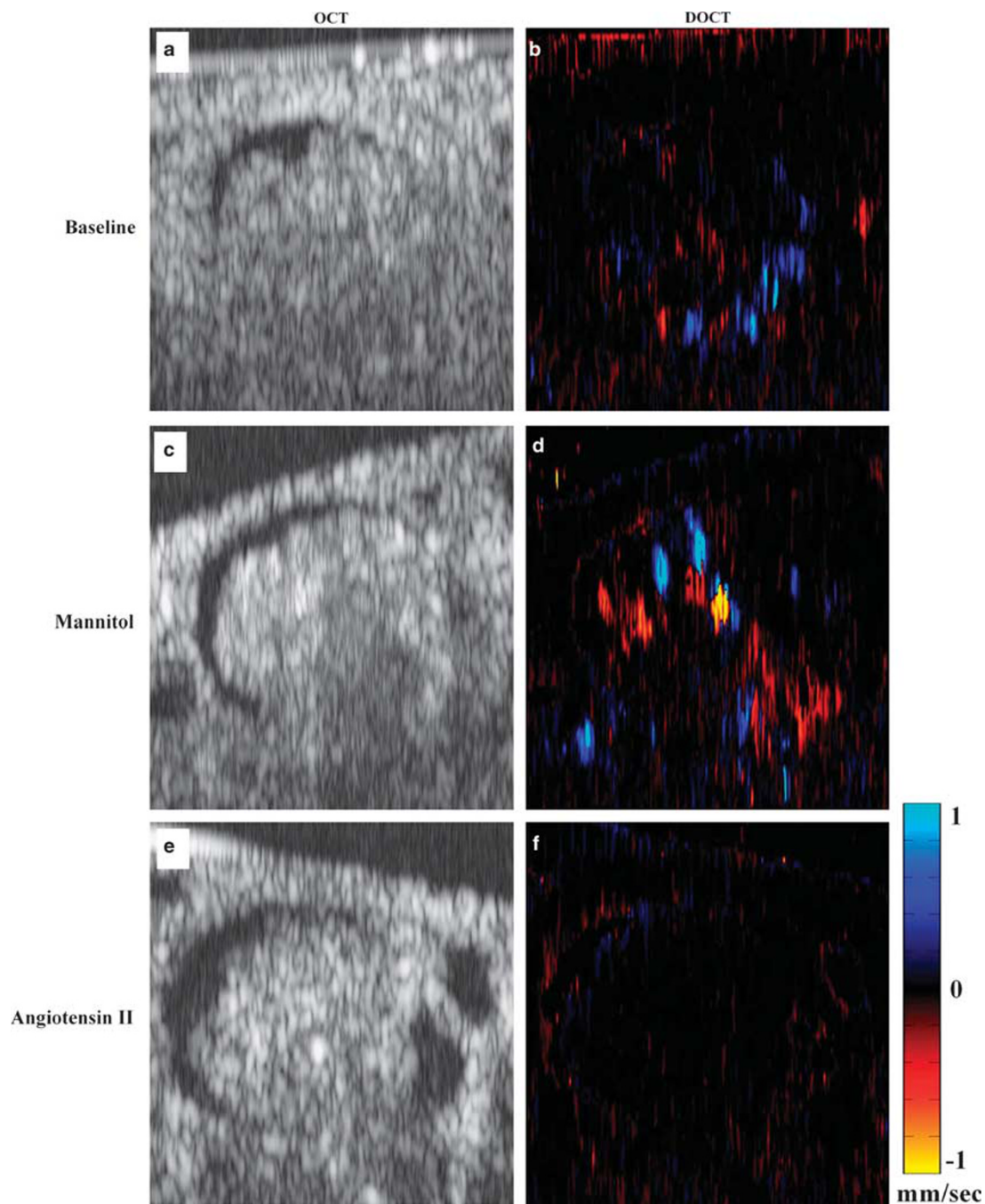


Figure 3 Representative OCT and DOCT images (XZ) from three different physiological states. (a, b) Baseline, (c, d) after mannitol, and (e, f) after angiotensin II. Comparison among the images shows differences in the observed DOCT signal in different glomeruli under altered blood flow conditions. Image size: $294 \times 278 \mu\text{m}$.

Analyzing 3D data sets enabled quantitative evaluation of the DOCT signal within the glomerular region. By segmenting the DOCT velocity signal at each depth position (*en face* plane) with a minimum background threshold ($|v_z|=0.05$ mm/s) and multiplying by the *en face* area of the segmented signal, blood flow histograms of the 3D DOCT data sets were obtained. Figure 4a shows a representative baseline blood flow histogram from the 3D DOCT imaging with Figure 4b showing close-up view of histogram base (region below dashed line). Similarly, Figures 4c and d shows a representative blood flow histogram after injection of mannitol solution and Figures 4e and f after injection of angiotensin II. The histogram peak following injection of mannitol increased to three times higher than the baseline histogram peak. This indicates that cumulative Doppler volume increased dramatically after administering mannitol (a mild vasodilator), and also, the maximum blood flow rate increased as noted by the wider range of flow rates (both positive and negative) as seen in Figure 4d (arrows) that are absent in the baseline histogram. Blood flow resulting after injection of angiotensin II (a vasoconstrictor) was also significantly affected. Figures 4e and f show flow rates only within one or two of the lowest histogram bins depicting a noticeable decrease of overall blood flow.

Three-dimensional (3D) analysis of OCT and DOCT data sets was performed to extract the total GV, DFR, and cumulative Doppler volume (CDV).

Figure 5 shows the computed GV, DFR, and CDV from one representative rat kidney. Figure 5a shows the GV from each of the seven physiological states induced during the experiment. Even though a slight increase in GV was noticed after injecting mannitol the first time and a slight decrease after injecting angiotensin II, no significant change in GV was observed during all data sets collected. Figure 5b and c shows the DFR and CDV values from the seven different physiological states in the same rat. For each state, an average of

$n \approx 4$ glomeruli were analyzed. It is interesting to note that after both the first and second mannitol injection, the DFR and CDV values returned to near-baseline levels during the 'recover' period indicating that the effects of the mannitol were wearing off (~ 15 – 20 min elapsed since injection). Shortly after administering the third mannitol injection to increase blood flow (10 min), angiotensin II was injected. This injection of angiotensin II reduced both DFR and CDV dramatically, well below the baseline level, even against the opposing effects of mannitol.

DISCUSSION

Optical imaging using DOCT, a functional extension of OCT, is able to reveal single glomerular blood flow *in vivo*. It is important to note that all the observations were performed without introducing artifacts otherwise associated with penetrating the kidney (ie, performed in a non-invasive fashion). Furthermore, DOCT requires no exogenous contrast agents like multi-photon fluorescence microscopy^{28,29,59} and confocal laser scanning microscopy⁶⁰ and offers deeper tissue penetration than most optical microscopy techniques. Although DOCT can penetrate to a depth of about ~ 1 – 2 mm, monitoring renal microcirculation < 500 μm below the kidney surface following renal transplantation has been reported to yield a promising predictive marker for post-transplant graft function.⁶¹ An additional advantage of DOCT is that it can acquire numerous cross-sectional images in rapid succession yielding comprehensive 3D volumes of tissue. Such images can be used to determine the size, shape, and blood flow through glomeruli, thereby providing pathological information regarding glomerular disease. Fast imaging speed⁶² and also the ability to be incorporated into needle^{63,64} and laparoscopic⁶⁵ devices for imaging blood flow in various orientations and even deeper in solid tissue or in not easily assessable locations allows DOCT to perform quick, repetitive 3D scans that can provide

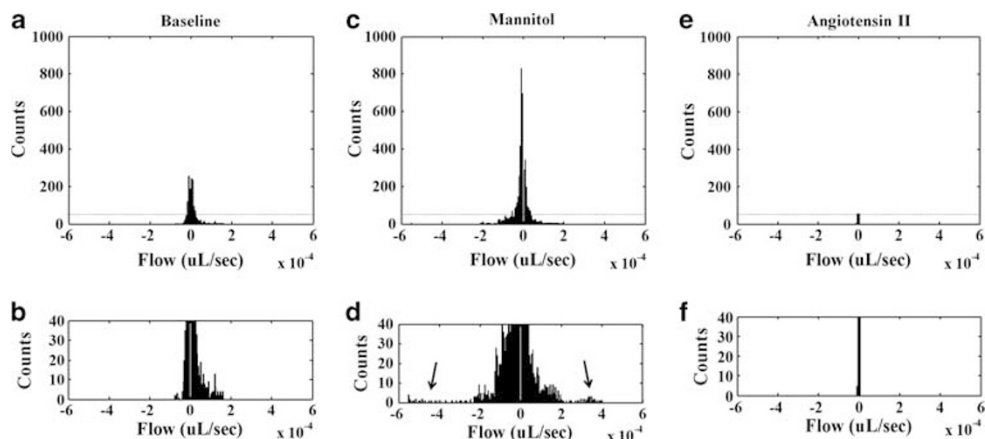


Figure 4 Blood flow histogram comparison. (a, b) Baseline blood flow histogram. (c, d) Blood flow histogram following injection of mannitol. (e, f) Blood flow histogram following injection of angiotensin II. Each histogram represents a compilation of the segmented DOCT signal at every *en face* plane through the depth of the glomerulus. Plots on the lower row are close-up versions at the base of the histograms (below the dashed line) in the upper row. Each group (a, b), (c, d), and (e, f) represents different glomeruli imaged in the same rat.

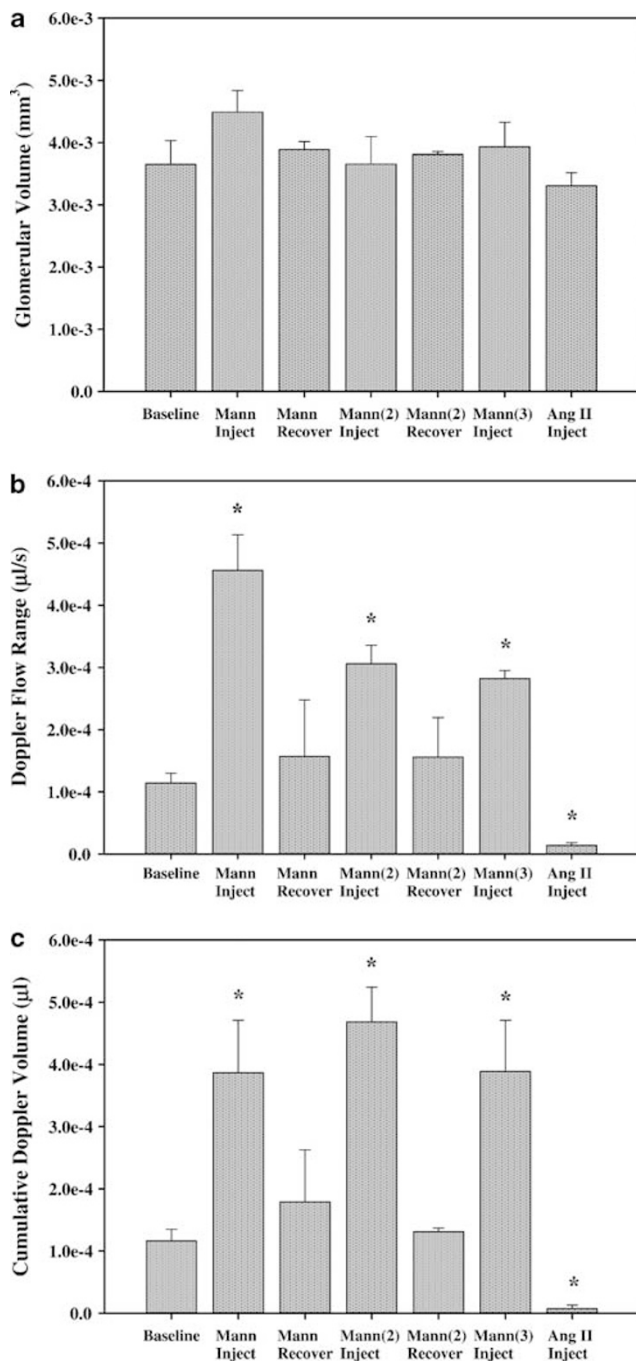


Figure 5 Analysis of *in vivo* DOCT imaging of rat glomeruli. (a) Glomerular volume. (b) Doppler flow range. (c) Cumulative Doppler volume. Each of these parameters was measured in multiple glomeruli under seven separate conditions: baseline ($n = 3$), following IV injection of mannitol ($n = 3$), after the effects of mannitol diminished ($n = 4$), following a second IV injection of mannitol ($n = 3$), after the effects of mannitol diminished ($n = 3$), following a third IV injection of mannitol ($n = 3$), and finally following an IV injection of angiotensin II ($n = 6$). Asterisk (*) indicates $P < 0.05$ compared with 'baseline'. Labels: Mann = mannitol; Ang II = angiotensin II.

vital information for kidney evaluation. These unique aspects of DOCT might make this imaging technology useful in clinical settings.

In our study, we demonstrated the ability of DOCT to quantitatively image glomerular blood flow *in vivo*. Blood cell velocities (between ± 1 mm/s) obtained with DOCT agree well with previous optical imaging studies^{21,60} as well as capillary blood flow ($\sim 1\text{--}4 \times 10^{-4}$ $\mu\text{l/s}$) as compared with values reported in the rat cerebral cortex.⁵⁸ However, DOCT quantifies velocity by detecting phase difference and therefore has an inherent phase-wrapping effect (as phase detection is limited by $\pm \pi$). The maximum detectable velocity (without phase-wrapping) is determined by the axial scan speed⁶⁶ and the minimum is based on the inherent phase noise present from the laser. In our system, 16 kHz axial scan speed yields our upper detection limit of ± 3.90 mm/s with minimum limit of ± 0.01 mm/s, which encompasses reported values of intra-glomerular blood flow. However, when imaging blood flow in arterioles, phase wrapping effect might be present (see Figure 1h). Future studies using higher-speed laser source^{62,66} would solve this limitation.

One limitation involved in the DOCT signal segmentation is the fact that the intra-glomerular capillaries are at or below the axial resolution of our system and therefore speckle noise might be a significant factor affecting quantification of the DOCT signal. As the segmented DOCT signal is composed of numerous small DOCT clusters representing the small vessels within the glomerulus, a large number of the voxels are boundary voxels and thus may only represent partially filled voxels. Some of the partial voxel effects might be alleviated by de-speckling but all the values we reported were calculated directly from the raw segmented DOCT signal before any image processing. Correction method for the possible error accrued from incomplete voxels is under investigation.

Furthermore, if the vascular pattern is of more interest, other techniques such as Doppler variance imaging,⁴¹ speckle variance imaging,⁶⁷ optical coherence angiography,⁶⁸ and optical microangiography⁶⁹ can be applied. Future studies are also needed to cross-validate the blood flow measured by DOCT with confocal or two-photon microscopy by using multi-modal optical systems.^{70–73}

Characterization of the captured 3D Doppler signal within the GV by the CDV and DFR metrics can relate the Doppler magnitude and spatial volume observed in each glomerulus. Although these two parameters are not sensitive to the same criteria, changes in capillary size/quantity and in flow speed will be detected by employing both in data analysis. For example, if the flow were to double while the capillaries remained the same size, the DFR would change accordingly but the CDV would remain constant. Likewise, if the number or size of the capillaries would change but the DFR did not, the CDV would indicate this change. By using both DFR and CDV metrics, alterations in the distribution (height or width) of the flow histogram can be detected and monitored for the 3D DOCT signal in each glomerulus.

Although the Munich–Wistar rat model provides superficial glomeruli that can be readily observed, the capability of DOCT to detect glomerular blood flow in the human kidney

has yet to be demonstrated. Previous studies show the ability of OCT to image glomeruli in the intact human kidney *ex vivo*^{36,37} and several of the studies mentioned above report using optical imaging methods at depths much shallower than DOCT to monitor renal circulation in animal models and transplant patients. Therefore, future studies using DOCT to quantify microcirculation changes compared with immediate and long-term transplant outcome and compared with renal disease progression would provide needed insights regarding possible future clinical applications of DOCT. However, the sensitivity of DOCT to detect subtle changes that can be associated with disease states (such as diabetes or renal artery stenosis) or with abnormal states (such as anemia or partial/full nephrectomy) has not yet been demonstrated.⁷⁴ Thus, further studies are needed to evaluate native blood flow responses to renal disease in animal models and human patients in order to better understand the capability of OCT/DOCT to provide quantitative measurements of the kidney.

In these studies, we have demonstrated 3D, label-free imaging of microcirculation in the rat glomerulus *in vivo* under different physiological conditions using DOCT. A significant difference in DFR and CDV was observed following injection of both mannitol and angiotensin II. The ability of DOCT to visualize hemodynamic changes *in vivo* could provide a direct method for clinicians to evaluate kidney perfusion and response to therapy in real time. Furthermore, intraoperative visualization and analysis of alterations in renal perfusion associated with injury or disease may help improve renal health care in the future.

Supplementary Information accompanies the paper on the Laboratory Investigation website (<http://www.laboratoryinvestigation.org>)

ACKNOWLEDGEMENTS

This work is supported in part by the Nanobiotechnology Award of the State of Maryland, the Minta Martin Foundation, the Prevent Cancer Foundation, the UMB-UMCP SEED Grant Program, the A. Ward Ford Memorial Research Grant, and NIH R21-EB012215.

DISCLOSURE/CONFLICT OF INTEREST

The authors declare no conflict of interest.

- Ogasawara Y, Takehara K, Yamamoto T, et al. Quantitative blood velocity mapping in glomerular capillaries by *in vivo* observation with an intravital videomicroscope. *Methods Inf Med* 2000;39:175–178.
- Ibrahim HN, Hostetter TH. Diabetic nephropathy. *J Am Soc Nephrol* 1997;8:487–493.
- O'Bryan GT, Hostetter TH. The renal hemodynamic basis of diabetic nephropathy. *Semin Nephrol* 1997;17:93–100.
- Ichikawa I, Fogo A. Focal segmental glomerulosclerosis. *Pediatr Nephrol* 1996;10:374–391.
- Szabo Z, Xia J, Mathews WB, et al. Future direction of renal positron emission tomography. *Semin Nucl Med* 2006;36:36–50.
- Juillard L, Janier MF, Fouque D, et al. Dynamic renal blood flow measurement by positron emission tomography in patients with CRF. *Am J Kidney Dis* 2002;40:947–954.
- Kudomi N, Koivuviita N, Liukko KE, et al. Parametric renal blood flow imaging using [¹⁵O]H₂O and PET. *Eur J Nucl Med Mol Imaging* 2009;36:683–691.
- Nitzsche EU, Choi Y, Killion D, et al. Quantification and parametric imaging of renal cortical blood flow *in vivo* based on Patlak graphical analysis. *Kidney Int* 1993;44:985–996.
- Middlekauff HR, Nitzsche EU, Nguyen AH, et al. Modulation of renal cortical blood flow during static exercise in humans. *Circ Res* 1997;80:62–68.
- Alpert NM, Rabito CA, Correia DJ, et al. Mapping of local renal blood flow with PET and H(2)(15)O. *J Nucl Med* 2002;43:470–475.
- Michoux N, Montet X, Pechere A, et al. Parametric and quantitative analysis of MR renographic curves for assessing the functional behaviour of the kidney. *Eur J Radiol* 2005;54:124–135.
- Vallee JP, Lazeyras F, Khan HG, et al. Absolute renal blood flow quantification by dynamic MRI and Gd-DTPA. *Eur Radiol* 2000;10:1245–1252.
- Bokacheva L, Rusinek H, Zhang JL, et al. Assessment of renal function with dynamic contrast-enhanced MR imaging. *Magn Reson Imaging Clin N Am* 2008;16:597–611, viii.
- De Bazelaire C, Rofsky NM, Duhamel G, et al. Arterial spin labeling blood flow magnetic resonance imaging for the characterization of metastatic renal cell carcinoma(1). *Acad Radiol* 2005;12:347–357.
- Akinbi H, Abbasi S, Hilpert PL, et al. Gastrointestinal and renal blood flow velocity profile in neonates with birth asphyxia. *J Pediatr* 1994;125:625–627.
- van Bel F, Guit GL, Schipper J, et al. Indomethacin-induced changes in renal blood flow velocity waveform in premature infants investigated with color Doppler imaging. *J Pediatr* 1991;118(Part 1):621–626.
- Wong SN, Lo RN, Yu EC. Renal blood flow pattern by noninvasive Doppler ultrasound in normal children and acute renal failure patients. *J Ultrasound Med* 1989;8:135–141.
- Yura T, Yuasa S, Fukunaga M, et al. Role for Doppler ultrasound in the assessment of renal circulation: effects of dopamine and dobutamine on renal hemodynamics in humans. *Nephron* 1995;71:168–175.
- Kalantarinia K, Belcik JT, Patrie JT, et al. Real-time measurement of renal blood flow in healthy subjects using contrast-enhanced ultrasound. *Am J Physiol Ren Physiol* 2009;297:F1129–F1134.
- Kay DH, Mazonakis M, Geddes C, et al. Ultrasonic microbubble contrast agents and the transplant kidney. *Clin Radiol* 2009;64:1081–1087.
- Yamamoto T, Tada T, Brodsky SV, et al. Intravital videomicroscopy of peritubular capillaries in renal ischemia. *Am J Physiol Renal Physiol* 2002;282:F1150–F1155.
- Angelescu M, Kraus T, Wiesel M, et al. Assessment of renal graft function by perioperative monitoring of cortical microcirculation in kidney transplantation. *Transplantation* 2003;75:1190–1196.
- Anaise D, Oster ZH, Atkins HL, et al. Cortex perfusion index: a sensitive detector of acute rejection crisis in transplanted kidneys. *J Nucl Med* 1986;27:1697–1701.
- Hamilton D, Miola UJ, Payne MC. The renal transplant perfusion index: reduction in the error and variability. *Eur J Nucl Med* 1994;21:232–238.
- Andrews PM, Petroll WM, Cavanagh HD, et al. Tandem scanning confocal microscopy (TSCM) of normal and ischemic living kidneys. *Am J Anat* 1991;191:95–102.
- Andrews PM, Khirabadi BS, Bengs BC. Using tandem scanning confocal microscopy to predict the status of donor kidneys. *Nephron* 2002;91:148–155.
- Campo-Ruiz V, Lauwers GY, Anderson RR, et al. Novel virtual biopsy of the kidney with near infrared, reflectance confocal microscopy: a pilot study *in vivo* and *ex vivo*. *J Urol* 2006;175:327–336.
- Kang JJ, Toma I, Sipsos A, et al. Quantitative imaging of basic functions in renal (patho)physiology. *Am J Physiol Renal Physiol* 2006;291:F495–F502.
- Dunn KW, Sandoval RM, Kelly KJ, et al. Functional studies of the kidney of living animals using multicolor two-photon microscopy. *Am J Physiol Cell Physiol* 2002;283:C905–C916.
- Yu W, Sandoval RM, Molitoris BA. Rapid determination of renal filtration function using an optical ratiometric imaging approach. *Am J Physiol Renal Physiol* 2007;292:F1873–F1880.
- Clark AL, Gillenwater A, Alizadeh-Naderi R, et al. Detection and diagnosis of oral neoplasia with an optical coherence microscope. *J Biomed Opt* 2004;9:1271–1280.
- Huang D, Swanson EA, Lin CP, et al. Optical coherence tomography. *Science* 1991;254:1178–1181.
- Chen Z, Milner TE, Srinivas S, et al. Noninvasive imaging of *in vivo* blood flow velocity using optical Doppler tomography. *Opt Lett* 1997;22:1119–1121.

34. Chen Y, Andrews PM, Aguirre AD, *et al*. High-resolution three-dimensional optical coherence tomography imaging of kidney microanatomy *ex vivo*. *J Biomed Opt* 2007;12:034008.
35. Andrews PM, Chen Y, Onozato ML, *et al*. High-resolution optical coherence tomography imaging of the living kidney. *Lab Invest* 2008;88:441–449.
36. Li Q, Onozato ML, Andrews PM, *et al*. Automated quantification of microstructural dimensions of the human kidney using optical coherence tomography (OCT). *Opt Express* 2009;17:16000–16016.
37. Onozato ML, Andrews PM, Li Q, *et al*. Optical coherence tomography of human kidney. *J Urol* 2010;183:2090–2094.
38. Tojo A. Optical coherence tomography in the kidney: a step toward echo microscopy. *J Urol* 2010;183:1669–1670.
39. Yang VXD, Gordon M, Qi B, *et al*. High speed, wide velocity dynamic range Doppler optical coherence tomography (Part I): System design, signal processing, and performance. *Opt Express* 2003;11:794–809.
40. Yazdanfar S, Rollins AM, Izatt JA. Imaging and velocimetry of the human retinal circulation with color Doppler optical coherence tomography. *Opt Lett* 2000;25:1448–1450.
41. Yu L, Chen Z. Doppler variance imaging for three-dimensional retina and choroid angiography. *J Biomed Opt* 2010;15:016029.
42. Wang Y, Bower BA, Izatt JA, *et al*. Retinal blood flow measurement by circumpapillary Fourier domain Doppler optical coherence tomography. *J Biomed Opt* 2008;13:064003.
43. Werkmeister RM, Dragostinoff N, Pircher M, *et al*. Bidirectional Doppler fourier-domain optical coherence tomography for measurement of absolute flow velocities in human retinal vessels. *Opt Lett* 2008;33:2967–2969.
44. Barton J, Izatt JA, Kulkarni MD, *et al*. Three-dimensional reconstruction of blood vessels from *in vivo* color Doppler optical coherence tomography images. *Dermatology* 1999;198:355–361.
45. Zhao Y, Chen Z, Saxer C, *et al*. Doppler standard deviation imaging for clinical monitoring of *in vivo* human skin blood flow. *Opt Lett* 2000;25:1358–1360.
46. Li H, Standish BA, Mariampillai A, *et al*. Feasibility of interstitial Doppler optical coherence tomography for *in vivo* detection of microvascular changes during photodynamic therapy. *Lasers Surg Med* 2006;38:754–761.
47. Yang VXD, Tang SJ, Gordon ML, *et al*. Endoscopic Doppler optical coherence tomography in the human GI tract: initial experience. *Gastrointest Endosc* 2005;61:879–890.
48. Hackbarth H, Buttner D, Jarck D, *et al*. Distribution of glomeruli in the renal cortex of Munich Wistar Fromter (MWF) rats. *Ren Physiol* 1983;6:63–71.
49. Stahl WM. Effect of Mannitol on the Kidney: Changes in Intrarenal Hemodynamics. *N Engl J Med* 1965;272:382–386.
50. Lindstrom KE, Ronnstedt L, Jaremko G, *et al*. Physiological and morphological effects of perfusing isolated rat kidneys with hyperosmolar mannitol solutions. *Acta Physiol Scand* 1999;166:231–238.
51. Behnia R, Koushanpour E, Brunner EA. Effects of hyperosmotic mannitol infusion on hemodynamics of dog kidney. *Anesth Analg* 1996;82:902–908.
52. Deng X, Welch WJ, Wilcox CS. Role of nitric oxide in short-term and prolonged effects of angiotensin II on renal hemodynamics. *Hypertension* 1996;27:1173–1179.
53. Ekelund L, Gothlin J. Effect of angiotensin on normal renal circulation determined by angiography and a dye dilution technique. *Acta Radiol Diagn (Stockh)* 1977;18:39–48.
54. Gothlin JH, Krakenes J, Tvette S. The effects of angiotensin on the diagnostics and haemodynamics in renal angiography. *Eur J Radiol* 1983;3:328–330.
55. Hall JE, Granger JP. Renal hemodynamic actions of angiotensin II: interaction with tubuloglomerular feedback. *Am J Physiol* 1983;245:R166–R173.
56. Denton KM, Anderson WP, Sinniah R. Effects of angiotensin II on regional afferent and efferent arteriole dimensions and the glomerular pole. *Am J Physiol Regul Integr Comp Physiol* 2000;279:R629–R638.
57. Yang VXD, Gordon M, Tang SJ, *et al*. High speed, wide velocity dynamic range Doppler optical coherence tomography (Part III): *in vivo* endoscopic imaging of blood flow in the rat and human gastrointestinal tracts. *Opt Express* 2003;11:2416–2424.
58. Srinivasan VJ, Sakadzic S, Gorczynska I, *et al*. Quantitative cerebral blood flow with optical coherence tomography. *Opt Express* 2010;18:2477–2494.
59. Molitoris BA, Sandoval RM. Intravital multiphoton microscopy of dynamic renal processes. *Am J Physiol Renal Physiol* 2005;288:F1084–F1089.
60. Li B, Yao J, Kawamura K, *et al*. Real-time observation of glomerular hemodynamic changes in diabetic rats: effects of insulin and ARB. *Kidney Int* 2004;66:1939–1948.
61. Schmitz V, Schaser KD, Olschewski P, *et al*. *In vivo* visualization of early microcirculatory changes following ischemia/reperfusion injury in human kidney transplantation. *Eur Surg Res* 2008;40:19–25.
62. Adler DC, Chen Y, Huber R, *et al*. Three-dimensional endomicroscopy using optical coherence tomography. *Nat Photonics* 2007;1:709–716.
63. Li X, Chudoba C, Ko T, *et al*. Imaging needle for optical coherence tomography. *Opt Lett* 2000;25:1520–1522.
64. Yang VXD, Mao YX, Munce N, *et al*. Interstitial Doppler optical coherence tomography. *Opt Lett* 2005;30:1791–1793.
65. Hariiri LP, Bonnema GT, Schmidt K, *et al*. Laparoscopic optical coherence tomography imaging of human ovarian cancer. *Gynecol Oncol* 2009;114:188–194.
66. Wieser W, Biedermann BR, Klein T, *et al*. Multi-megahertz OCT: High quality 3D imaging at 20 million A-Scans and 4.5 GVoxels per second. *Opt Express* 2010;18:14685–14704.
67. Mariampillai A, Leung MK, Jarvi M, *et al*. Optimized speckle variance OCT imaging of microvasculature. *Opt Lett* 2010;35:1257–1259.
68. Makita S, Hong Y, Yamanari M, *et al*. Optical coherence angiography. *Opt Express* 2006;14:7821–7840.
69. Zhi Z, Jung Y, Jia Y, *et al*. High sensitive imaging of renal microcirculation *in vivo* using ultrahigh sensitive optical microangiography. *Biomed Opt Express* 2011;2:1059–1068.
70. Chen CW, Betz MW, Fisher JP, *et al*. Macroporous hydrogel scaffolds and their characterization by optical coherence tomography. *Tissue Eng: Part C* 2011;17:101–112.
71. Dunkers J, Cicerone M, Washburn N. Collinear optical coherence and confocal fluorescence microscopies for tissue engineering. *Opt Express* 2003;11:3074–3079.
72. Tang S, Sun CH, Krasieva TB, *et al*. Imaging subcellular scattering contrast by using combined optical coherence and multiphoton microscopy. *Opt Lett* 2007;32:503–505.
73. Vinegoni C, Ralston T, Tan W, *et al*. Integrated structural and functional optical imaging combining spectral-domain optical coherence and multiphoton microscopy. *Appl Phys Lett* 2006;88:053901.
74. Regan MC, Young LS, Geraghty J, *et al*. Regional renal blood flow in normal and disease states. *Urol Res* 1995;23:1–10.